Anomalous sound attenuation in the metal-nonmetal transition range of liquid mercury

1999 J. Phys.: Condens. Matter 11 5399

(http://iopscience.iop.org/0953-8984/11/28/302)

J. Phys.: Condens. Matter **11** (1999) 5399–5413. Printed in the UK PII: S0953-8984(99)02664-8

Anomalous sound attenuation in the metal–nonmetal transition range of liquid mercury

H Kohno and M Yao†

Department of Physics, Graduate School of Science, Kyoto University, Sakyo-ku 606-8502, Kyoto, Japan

E-mail: yao@scphys.kyoto-u.ac.jp

Received 16 March 1999, in final form 28 April 1999

Abstract. The sound velocity, v, and the sound attenuation coefficient, α, of fluid mercury have been measured at 20 MHz in the temperature and pressure range up to 1600 °C and 200 MPa. To obtain the precise sound attenuation data under high temperature and pressure, we have derived the formula for estimating α by taking into account the sound absorption in the buffer rods and the acoustic impedance mismatches between the buffer rods and the sample Hg. The measurements have been carried out with four different sample lengths, and the agreements among these measurements are fairly good in the common density range. Beside the critical attenuation of sound propagation, we have observed the secondary maximum in the density dependence of α at a density near 9 g cm^{-3}, where the metal–nonmetal (M–NM) transition occurs. In contrast to the critical attenuation, the height of the secondary maximum is almost independent of temperature. Assuming a Debye-type relaxation for the frequency-dependent adiabatic compressibility, we have estimated the relaxation time from the anomalous attenuation. We conclude that in expanded liquid Hg slow dynamics is generated by the sound pressure in the M–NM transition range.

1. Introduction

Since the liquid–gas critical point of mercury is located at relatively low temperature (= 1478 °C) and pressure (= 167 MPa), various physical properties have been investigated experimentally in a wide density range including the supercritical conditions. The studies on the electronic properties such as the optical properties [1–4], transport properties [5–8] and magnetic properties [9, 10] have revealed that a metal–nonmetal (M–NM) transition occurs at densities 8 to 9 g cm^{-3}, which is appreciably larger than the critical density (5.8 g cm^{-3}). These experimental studies have stimulated many theoretical works. Mattheiss and Warren [11] performed a band structure calculation for several hypothetical forms of crystalline Hg with fixed nearest neighbour distance to model the density variation of the density of states at the Fermi energy, E_F, in expanded fluid Hg. When the density decreases, the calculated s-electron component of the density of states at E_F vanishes at a considerably smaller density than the Knight shift [10]. Then, they had to elongate the nearest neighbour distance by 4% to reproduce the experimental results. On the other hand, Franz [12] proposed that the correct density for the M–NM transition can be theoretically predicted by taking fluctuations in the coordination number into account. Kresse and Hafner [13] calculated the radial distribution functions and the density of states for expanded liquid Hg by means of *ab initio* computer simulations, and

† Corresponding author.

0953-8984/99/285399+15$30.00

reproduced the pair distribution functions experimentally obtained by Tamura and Hosokawa [14] and the density variation of the optical gap [3]. As expected from the experimental data [1–10] (see also figure 8), it has been concluded that the M–NM transition in liquid Hg is mainly due to the lack of overlapping between the 6s and 6p bands.

An issue of considerable interest is that the M–NM transitions in the liquid state are, in most cases, not purely electronic transitions but are accompanied by changes in the thermodynamic and structural properties [15]. For liquid Hg an anomalous density variation of the equation of state has been observed in the M–NM transition range [8]. In addition, the density variation of the sound velocity shows an inflection from a metallic branch to a nonmetallic one. This phenomenon was first observed by Suzuki *et al* [16], and confirmed by subsequent works [17–19]. Furthermore, the x-ray diffraction study by Tamura and Hosokawa [20] implies that the nearest neighbour distance is elongated by about 1% when the density decreases in the M–NM transition range. Theoretically Munejiri *et al* [21] have deduced effective pair-potentials from the experimental data by Tamura and Hosokawa [22] by means of the inverse problem and used them to reproduce the density dependence of the sound velocity.

All the studies mentioned above are mainly aimed at investigating the static properties of liquid Hg. Since the most characteristic feature of the liquid state, compared with the solid state, is the time evolution of the atomic arrangement, it would be very interesting to study dynamic aspects of the M–NM transition. For this purpose the measurement of the sound attenuation may be promising. Some years ago, we reported preliminary results of the sound attenuation for expanded liquid Hg [18]. We found that the attenuation becomes large at relatively high densities compared with the density variation for simple liquids such as Ar. We assigned the anomaly to the increase of the bulk viscosity and speculated that in the M–NM transition range it may take some relaxation time for the metallic domain, which is generated by the local compression, to be restored to a semiconducting domain. Kozhevnikov *et al* [23] also reported the extinction of the sound wave for fluid Hg.

Recently we have measured the sound velocity and attenuation of expanded liquid Hg in a wider temperature and pressure range [24] and obtained more extensive and more accurate data, from which we can draw a conclusion that both the sound velocity and the attenuation exhibit anomalous behaviours in the M–NM transition range. The major purpose of this paper is to present the new data on the sound attenuation of liquid Hg over a wide density range and to discuss a dynamic aspect of the M–NM transition for the first time.

The remainder of this paper is divided as follows. In section 2 we describe the experimental apparatus for the acoustic measurements and explain how to deduce the precise attenuation coefficient of liquid Hg under the high temperature and pressure conditions. Since the sound velocity data are necessary for deducing the attenuation coefficient, we present first the results of sound velocity and then the attenuation in section 3. Analysing the density dependence of the attenuation, we demonstrate that there appears a secondary maximum in the M–NM transition range. In section 4, assuming a Debye-type relaxation for the frequency-dependent adiabatic compressibility, we try to estimate the relaxation time corresponding to the anomalous attenuation due to the M–NM transition, and a possible model for the origin of the relaxation is discussed. Although we have also observed significant attenuation in the liquid–gas critical region, a detailed analysis of the critical attenuation will be described elsewhere [25]. Finally the summary is given in section 5.

2. Experimental procedure

The experimental apparatus for the ultrasonic measurements is shown in figure 1. Single crystalline sapphire rods 8 mm in diameter were used as buffer rods for transmitting the

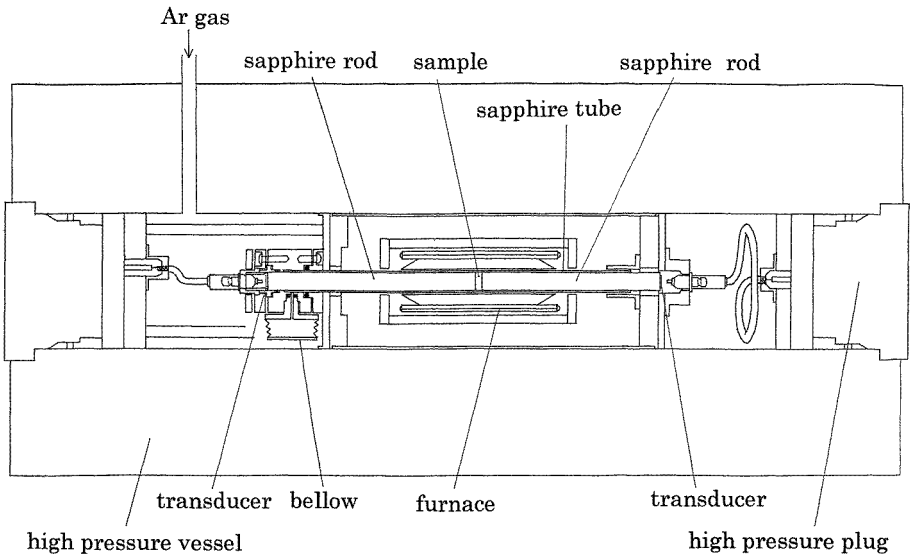

Figure 1. The experimental apparatus for measuring the sound velocity and attenuation.

ultrasonic waves. Two sapphire rods, A and B, were inserted into a single crystalline sapphire tube with the inner diameter of 8 mm and the outer diameter of 10 mm. The axial length of both sapphire rods was 89 mm. A gap between the two rods was the sample part and the sample lengths l_S were 0.30 mm, 0.98 mm, 1.90 mm and 7.00 mm. Hereafter we refer to these sample thicknesses as 0.3 mm, 1 mm, 2 mm and 7 mm, respectively, for brevity. A sample reservoir made of a stainless steel bellows was located at one cold end of the cell, and the Hg sample was introduced from the reservoir into the sample part through a clearance between the sapphire tube and the sapphire rod A. The sample cell was tightly sealed by glaze and viton O-rings, and the bellows served to equilibrate the pressure in the cell with the applied one. The temperature of the sample part was raised by two independently controlled heaters surrounding the central part of the cell, and monitored by two W–5% Re:W–26% Re thermocouples. The temperature was calibrated by using a saturated vapour pressure curve [26]. The cell assembly together with the two heaters were set in a steel high pressure vessel which was pressurized with argon gas. The inner and outer diameters of the high pressure vessel were 60 and 180 mm, respectively. The pressure was measured by a Heise gauge. The experimental errors in temperature and pressure were $\pm 3\,^{\circ}$C and ± 0.5 MPa, respectively.

The sound velocity, v, was measured by an ultrasonic pulse transmission/echo method [16, 18]. X-cut quartz or Z-cut Pb(Zr·Ti)O_3 transducers with the resonance frequency of 20 MHz were bonded to the cold ends of sapphire rods. The time required for an ultrasonic pulse to traverse from one transducer to the other, τ_{AB}, and the time required for an echo to return from the interface between the rod A (or B) and the sample, τ_{AA}(or τ_{BB}), were measured. All the signals were accumulated 100 times and recorded with a digital oscilloscope. The difference between τ_{AB} and $(\tau_{AA} + \tau_{BB})/2$ gives the time required for the pulse to traverse the sample. Then v can be deduced from

$$v = l_S/\{\tau_{AB} - (\tau_{AA} + \tau_{BB})/2\}. \tag{1}$$

The error of the sound velocity, v, was less than 3%.

The sound attenuation coefficient α can be deduced from

$$\alpha = -\ln T_S / l_S \tag{2}$$

where T_S is the transmission rate through the sample. In contrast to the ambient conditions, where T_S can be measured with varying sample thickness l_S, it is difficult to change l_S *in situ* under high temperature and pressure. Hence, we have estimated the transmission rate as follows.

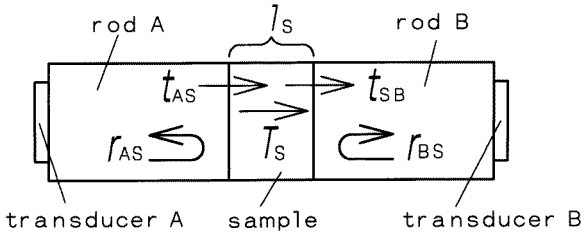

Figure 2. The schematic diagram of the experimental apparatus. Definitions of the transmissivity, t_{IJ}, and the reflectivity, r_{IJ}, at the interfaces are also shown. T_S is the transmission rate through the sample with a thickness of l_S.

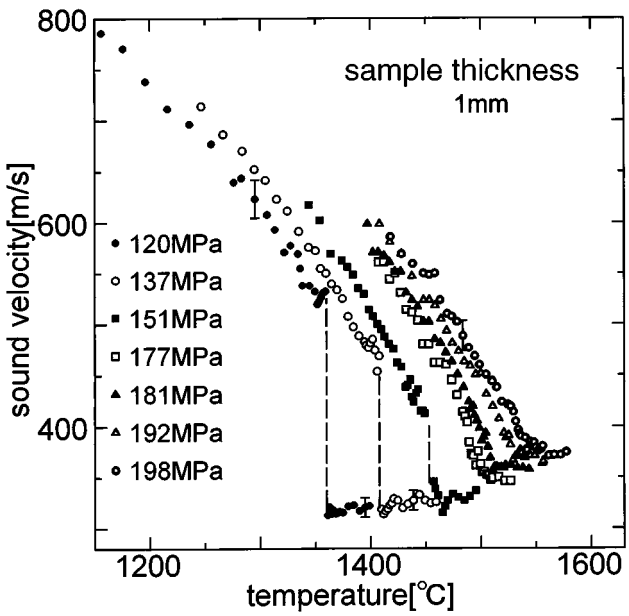

Figure 3. The sound velocity, v, along several experimental paths is shown as a function of temperature. Several different symbols are used depending on the pressure. The sample thickness was 1 mm.

When the incident pulse is applied to the transducer A, the sound pulse is transmitted through the rod A, sample and rod B successively, and reaches the transducer B (see figure 2). Here the voltage generated at the transducer B in this way is denoted by V_{AB}. Since fairly long buffer rods are necessary for the measurements at high temperatures, the sound attenuation due to the sapphire rods is no longer negligible. Therefore, we measured not only V_{AB} but

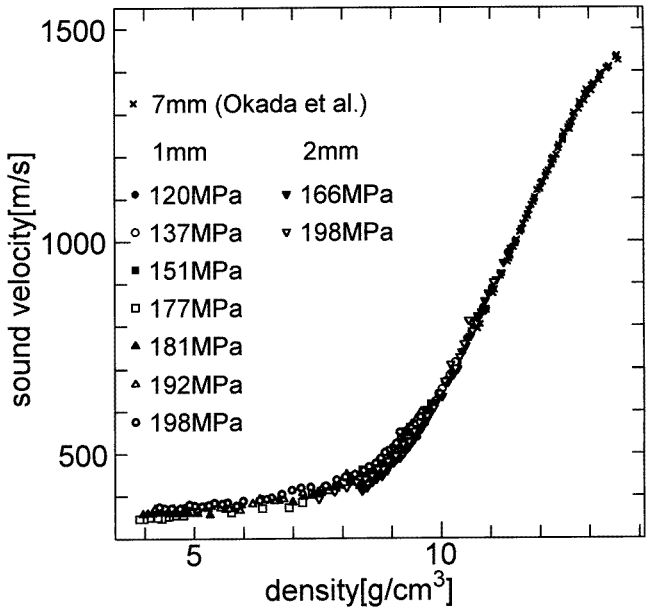

Figure 4. The sound velocity, v, is shown as function of density. Several different symbols are used depending on the pressure and the sample lengths. The meaning of these symbols is shown in the figure. The results for the sample length of 7 mm were measured by Okada *et al* [19].

also the voltages, V_{AA} and V_{BB} which are generated at the transducers A and B, respectively, by the echo signals reflected from the interface between the Hg sample and the buffer rods. These quantities may be expressed as follows:

$$V_{AB} = V_0\alpha_A T_A t_{AS} T_S t_{SB} T_B \beta_B \tag{3a}$$

$$V_{AA} = V_0\alpha_A T_A r_{AS} T_A \beta_A \tag{3b}$$

$$V_{BB} = V_0\alpha_B T_B r_{BS} T_B \beta_B \tag{3c}$$

where V_0 is the voltage of the incident pulse, and T_A (T_B) the transmission rate through the buffer rod A (B). $\alpha_A(\alpha_B)$ is the efficiency of the transducer A (B) in converting the electric voltage to the sound pressure, and $\beta_A(\beta_B)$ is the efficiency in the inverse process. $r_{AS}(r_{BS})$ is the reflectivity of the sound pressure at the interface between the buffer rod A (B) and the Hg sample, and $t_{AS}(t_{SB})$ is the transmissivity. The definition of $r_{AS}(r_{BS})$ and $t_{AS}(t_{SB})$ is illustrated in figure 2. These quantities can be calculated from

$$t_{IJ} = \frac{2z_J}{z_I + z_J} \tag{4a}$$

and

$$r_{IJ} = \frac{z_J - z_I}{z_I + z_J} \tag{4b}$$

where z_I is the acoustic impedance of the medium I and is expressed by the density ρ_I and the sound velocity v_I as

$$z_I = \rho_I v_I. \tag{5}$$

Making use of equations (3*a*), (3*b*) and (3*c*), one can deduce the following formula for the transmission rate T_S through the sample:

$$T_S = \frac{V_{AB}}{\sqrt{V_{AA}V_{BB}}} \frac{\sqrt{|r_{AS}||r_{BS}|}}{|t_{AS}||t_{SB}|} \sqrt{\frac{\alpha_B \beta_A}{\alpha_A \beta_B}}. \tag{6}$$

In the present paper we assume that the last term of equation (6), (i.e. $\sqrt{\alpha_B\beta_A/\alpha_A\beta_B}$) is unity. In principle the validity of this assumption is based upon the reciprocity of the conversion processes between the voltage and the sound pressure. In practice, however, it relies also upon the efficiency in bonding the transducer. Hence we bonded the transducers onto the sapphire surfaces as tightly as possible so that the reflected signals V_{AA} and V_{BB} could be optimized. We have measured the sound attenuation with four different sample thickness and compared the results of α deduced through the procedure mentioned above. We have confirmed that there are good agreements among the experiments (see section 3).

By using equation (2), the relative error of the attenuation coefficient, $|\Delta\alpha/\alpha|$, is expressed as follows,

$$\left|\frac{\Delta\alpha}{\alpha}\right| \leqslant \left|\frac{\Delta T_S}{T_S \ln T_S}\right| + \left|\frac{\Delta l_S}{l_S}\right|. \tag{7}$$

Here ΔT_S is the error of the transmission rate and Δl_S is the error of the sample thickness. From the scattering of data points, ΔT_S has been estimated to be ± 0.04 when T_S is about 0.7, and less than ± 0.02 when T_S is about 0.05. It is evident from the inequality (7) that the error limit of α becomes large not only when T_S approaches null but also when it approaches unity, indicating that only intermediate values of T_S are considered to be reliable. For the sample thickness of 1 mm or more, for which $|\Delta l_S/l|$ is less than 0.03, we have accepted the data when the T_S value lies between 0.05 and 0.7. For the sample thickness of 0.3 mm, for which $|\Delta l_S/l|$ is less than 0.08, we have adopted the T_S data between 0.06 and 0.6. Consequently the upper limit of the relative error of α is evaluated to be 20% throughout the present work.

3. Results and analysis

3.1. Sound velocity

The measurements of the sound velocity v and the attenuation coefficient α at 20 MHz were carried out for fluid Hg at nearly constant pressures. Figure 3 shows the results of v along several experimental paths for the Hg sample with 1 mm thickness as a function of temperature. In the figure, the number given to each symbol is the pressure at which the experimental path crosses the liquid–gas transition when the pressure is smaller than P_c (= 167 MPa), and it is the pressure at which the experimental path crosses the critical isochore line when $P > P_c$. Typical experimental uncertainties are indicated by the error bars. In the liquid state v decreases rapidly with increasing temperature, while it increases slowly with temperature in the gaseous state. Small undulations of v seen in the gaseous states are spurious, because the amplitude of such undulations are smaller than the typical error bars. At the liquid–gas transition v drops discontinuously to a small value. At 120 MPa, for example, the jump is seen near 1360 °C. We have observed no additional drop of v above the boiling point in contrast to the observation by Kozhevnikov *et al* [17, 23] who assigned the secondary drop to the prewetting transition at the interface between the molybdenum (or niobium) buffer rod and mercury sample [27]. Although the prewetting transition at the interface between mercury and sapphire is well established by several optical measurements [28, 29], it should be very difficult to detect the wetting transition by measuring the sound velocity, because the wetting layer is by far thinner than the sample

thickness. Except for the vicinity of the saturated vapour pressure curve, the present results of v are in good agreement with those by Kozhevnikov *et al* [17, 23].

The density dependence of the sound velocity v is shown in figure 4. The density has been determined by collecting the most accurate data on the isochore lines [8, 26, 30, 31]. The crosses denote the results of v measured by Okada *et al* [19] in a pressure range between 100 and 200 MPa for the sample length of 7 mm. At high densities the density is the most relevant parameter for determining the sound velocity and the pressure (or temperature) dependence of v at constant densities is small. As the density is decreased, the sound velocity decreases rapidly and near 9 g cm^{-3}, where the M–NM transition occurs, it becomes about one third of the value at the melting point. As first discovered by Suzuki *et al* [16] and confirmed by subsequent works [17–19], the density variation of v exhibits a clear inflection near the M–NM transition density. On the nonmetallic side v varies slowly with density and it exhibits appreciable pressure (or temperature) dependence. Representative numerical values of v are listed in table 1. The present results of v are in good agreement with the original results by Suzuki *et al* [16] at densities above 10 g cm^{-3}, and with the data by Dladla *et al* [32] below 8 g cm^{-3} within the experimental uncertainties.

Table 1. Sound velocity, v, and sound attenuation coefficient, α, of Hg.

Density [g cm^{-3}]	Temperature [°C]	Pressure [MPa]	v [m s^{-1}]	α [cm^{-1}]
5.0	1500	175.2	363 ± 11	18.4 ± 2.0
5.0	1513	180.5	367 ± 11	12.4 ± 1.3
5.0	1540	191.0	372 ± 11	8.17 ± 1.0
5.0	1555	196.5	378 ± 11	7.83 ± 0.9
6.0	1497	176.8	372 ± 11	79.2 ± 13.1
6.0	1506	181.2	376 ± 11	62.0 ± 9.9
6.0	1529	192.5	382 ± 11	25.7 ± 3.4
6.0	1540	198.3	389 ± 12	21.7 ± 2.5
7.0	1493	177.3	386 ± 12	46.5 ± 7.2
7.0	1501	182.3	392 ± 12	28.3 ± 4.7
7.0	1519	193.4	401 ± 12	18.3 ± 2.0
7.0	1530	199.8	414 ± 12	15.0 ± 1.6
8.0	1479	176.7	431 ± 13	15.6 ± 1.6
8.0	1488	183.5	436 ± 13	15.4 ± 1.6
8.0	1502	194.0	439 ± 13	14.2 ± 1.5
8.0	1512	201.0	443 ± 13	13.4 ± 1.4
9.0	1438	175.7	477 ± 14	12.0 ± 1.5
9.0	1448	184.0	479 ± 14	11.7 ± 1.4
9.0	1461	195.8	485 ± 15	11.6 ± 1.4
9.0	1470	203.7	488 ± 15	11.5 ± 1.4
10.0	1331	175.6	633 ± 19	5.80 ± 0.6
10.0	1343	187.8	636 ± 19	5.79 ± 0.6
10.0	1351	199.6	639 ± 19	5.65 ± 0.6
10.0	1362	205.6	641 ± 19	5.36 ± 0.6
11.0	1060	127.4	853 ± 26	2.53 ± 0.4
11.0	1087	164.7	874 ± 26	2.27 ± 0.4
11.0	1101	174.5	876 ± 26	2.26 ± 0.4
11.0	1117	201.8	881 ± 26	2.03 ± 0.4

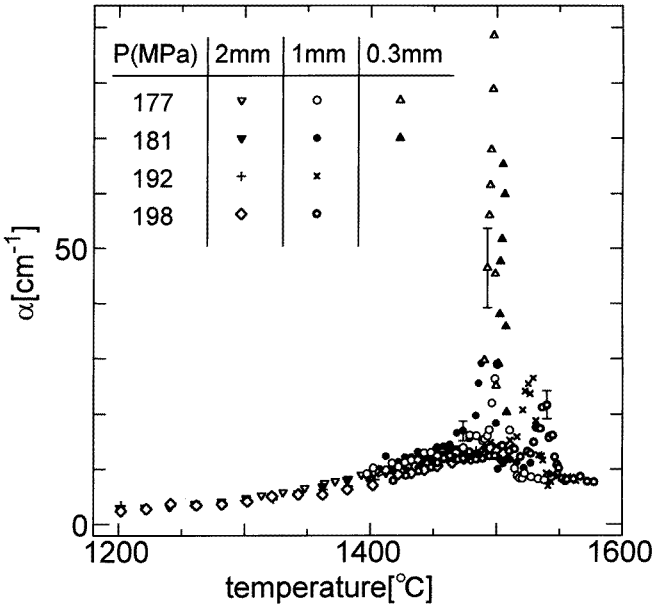

Figure 5. The attenuation coefficient, α, of a sound wave along several experimental paths is shown as a function of temperature. Several different symbols are used depending on the pressure and the sample lengths. The meaning of these symbols is tabulated in the figure.

3.2. Sound attenuation

The sound attenuation coefficient, α, at 20 MHz along several experimental paths are plotted in a wide temperature range in figure 5. The meaning of the various symbols is illustrated in a small table inserted in the figure. The table includes the pressures at which the experimental path crosses the critical isochore line and the sample lengths (0.3 mm, 1 mm and 2 mm). Typical experimental uncertainties are indicated by the error bars. The agreement among the data measured with different sample thickness is fairly good within the error limit of $\pm 20\%$. At low temperatures, α increases slowly with temperature and it increases rapidly above 1400 °C. Figure 6 shows the attenuation coefficient, α, around 1500 °C in an expanded scale. At constant pressures α has a maximum at the temperature on the critical isochore lines. At 177 MPa the peak is located at 1497 °C and its height is 88.5 ± 16.7 cm^{-1}. The peak becomes smaller as the pressure increases. That is, the peak height is 65.2 ± 10.5 cm^{-1} at 181 MPa and 1505 °C, 26.6 ± 3.6 cm^{-1} at 192 MPa and 1529 °C, and 21.7 ± 2.5 cm^{-1} at 198 MPa and 1540 °C.

The results of α at 177, 181, 192 and 198 MPa are plotted as a function of density in figures 7(a), (b), (c) and (d), respectively. The data for the sample lengths of 7 mm were taken by Okada *et al* [19]. When the density decreases, α begins to increase around 11 g cm^{-3}, and reaches a maximum near the critical density. The latter is a clear indication of the critical attenuation. In addition to the critical attenuation, it should be noticed that a *hump* appears in the α–ρ curves around 9 g cm^{-3}, where the M–NM transition occurs. The changes in α around 9 g cm^{-3} can be seen more clearly at pressures much higher than P_c, because the critical attenuation diminishes with increasing pressure. In figure 7(d) the *hump* around 9 g cm^{-3} is well resolved from the critical attenuation and becomes a clear secondary maximum.

The shape of the secondary maximum can be approximately fitted to a Gaussian function, as shown by the long-dashed lines in figure 7(d). The Gaussian function that has a peak value

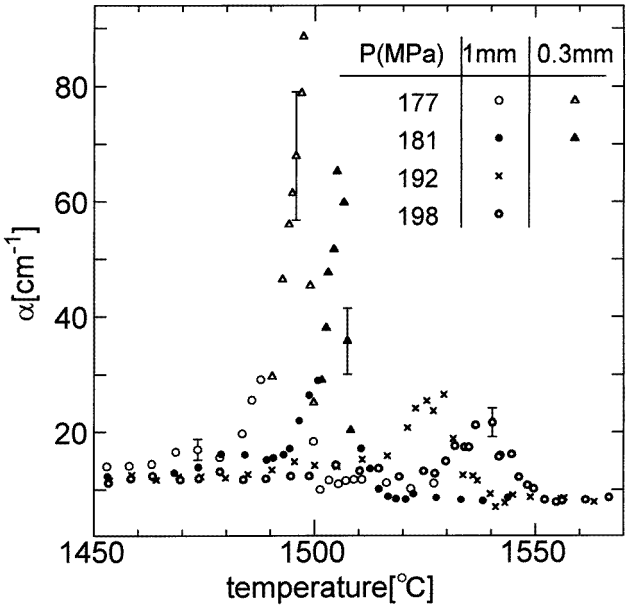

Figure 6. The attenuation coefficient, α, of a sound wave around 1500 °C is shown as a function of temperature. Several different symbols are used depending on the pressure and the sample lengths. The meaning of these symbols is tabulated in the figure.

of 12.9 cm^{-1} at the density ρ_{SM} of 8.3 g cm^{-3} with the standard deviation σ_{SM} of 1.2 g cm^{-3} reproduces the experimental points above 8.0 g cm^{-3} very well. The density variation of α at other pressures can be expressed by the same curve, as shown by the long-dashed lines in figures 7(a), (b), (c). These figures indicate that the shape of the secondary maximum is almost independent of pressure, that is, independent of temperature, because

$$\left(\frac{\partial\alpha}{\partial P}\right)_\rho = \left(\frac{\partial\alpha}{\partial T}\right)_\rho \left(\frac{\partial T}{\partial P}\right)_\rho \simeq 0. \tag{8}$$

This is in sharp contrast to the critical attenuation which depends strongly on pressure and hence on temperature. The short-dashed lines in figure 7 are guides for the eyes to the critical attenuation. The Gaussian function reproducing the density dependence of α in the M–NM transition range is also shown in figure 8 together with the density dependence of the NMR Knight shift [10] and the optical gap [4].

The numerical values of α are listed at various densities and temperatures in table 1.

4. Discussion

Except for the vicinity of the critical point, the sound attenuation in simple liquids may be described as [33]

$$\frac{\alpha}{f^2} = \frac{2\pi^2}{\rho v^3}\left\{(\zeta + \tfrac{4}{3}\eta) + \kappa\left(\frac{1}{C_v} - \frac{1}{C_p}\right)\right\} \tag{9}$$

where f is the frequency, ζ and η are the bulk and shear viscosities, respectively, κ is the thermal conductivity and C_v and C_p are the specific heats at constant volume and pressure, respectively. We discuss first the sound attenuation of Hg at high densities. In figure 9, the

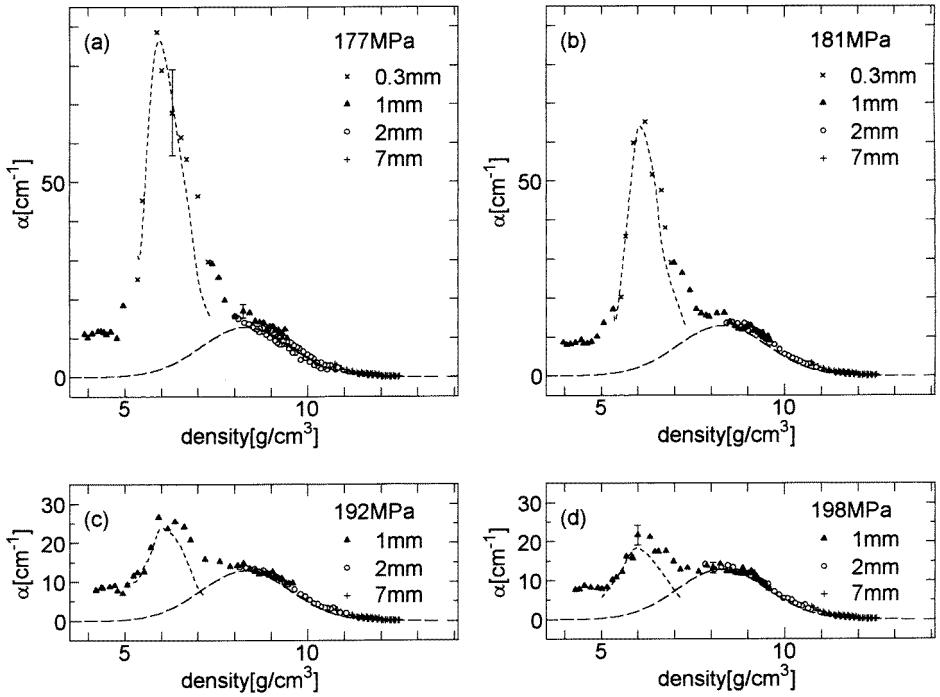

Figure 7. The attenuation coefficient, α, at 177 MPa (a), at 181 MPa (b), at 192 MPa (c) and at 198 MPa (d) is shown as a function of density. Four different symbols are used depending on the sample lengths. The results for the sample length of 7 mm were measured by Okada *et al* [19].

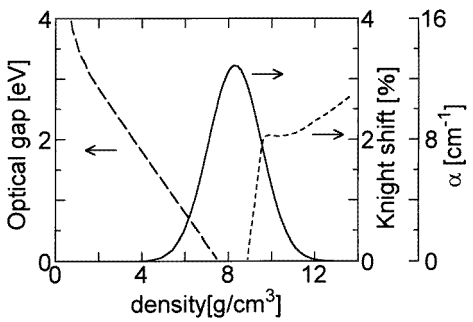

Figure 8. The secondary maximum in the density dependence of the attenuation coefficient, α, is shown by the solid line together with the density dependence of the optical gap [4] denoted by the long-dashed line and the Knight shift [10] denoted by the short-dashed line.

logarithm of α/f^2 at 120 MPa is shown as a function of density. The triangles denotes the results for the sample length of 1 mm, and the crosses denotes the results for 7 mm [19]. The density dependence of these results is well compatible with the α-values denoted by the open circles, which were measured by Hunter *et al* [34] at 90 MHz, though one must be careful because the relative experimental error in α, $\Delta\alpha/\alpha$, increases at high densities where α becomes small. We have estimated the shear viscosity contribution to α/f^2 from experimental values of η [35] as shown by the dashed line in figure 9. Compared with the measured α/f^2,

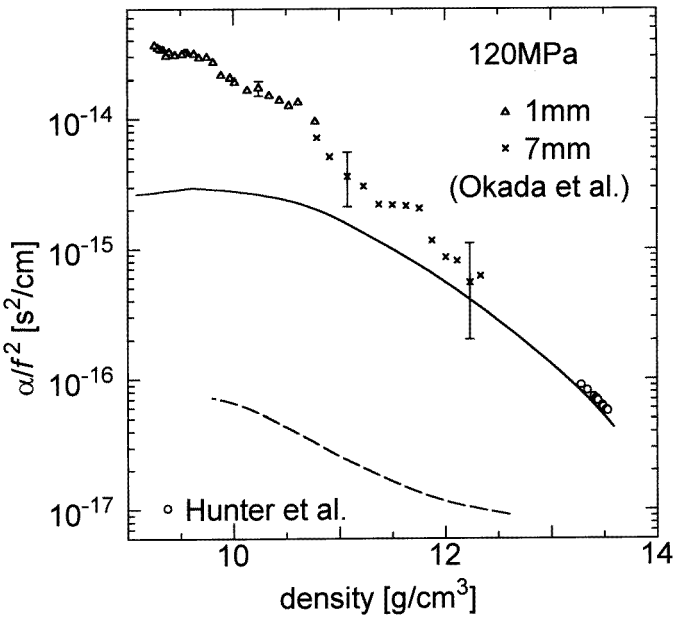

Figure 9. Logarithms of the attenuation coefficient divided by the square of frequency, α/f^2, at 120 MPa are plotted against the density. The crosses denotes the results for the sample length of 7 mm measured by Okada *et al* [19]. The dashed and solid lines denote the shear viscosity and thermal conductivity contributions to α/f^2, respectively. The open circles denote α/f^2 measured by Hunter *et al* at 90 MHz [34].

the shear viscosity term is negligibly small. The solid line in figure 9 denotes the thermal conductivity contribution to α/f^2. We have estimated κ from the electrical conductivity data [8] by using the Wiedemann–Franz relation [36]. The specific heats C_v and C_p are evaluated by combining the present sound velocity data with the most reliable *PVT* data [8, 26, 30, 31]. Unlike the early estimation of C_v and C_p from the sound velocity [8], the present values of C_v and C_p agree with those directly measured by Levin and Schmutzler [37]. Further details on the specific heats will be described elsewhere [38].

It is noticed in figure 9 that the experimental values of α/f^2 approximately give the thermal conductivity term in the high density range, indicating that the thermal conduction due to the conduction electrons plays the most dominant role in the sound attenuation in the high density range. This is consistent with an early suggestion, which was mainly based upon the experimental results of the Hall effect, that liquid Hg exhibits a nearly-free-electron behaviour at densities larger than 11 g cm^{-3}. On the other hand, at densities smaller than 11 g cm^{-3}, the sound attenuation is too large to be interpreted by the thermal conductivity term alone. At 10 g cm^{-3}, for example, the experimental α/f^2 is about seven times larger than the thermal conductivity term. Hence it is concluded from equation (9) that the increase of α at smaller densities should be associated with an increase in the bulk viscosity.

In general the bulk viscosity becomes important when the volume change occurs out of phase with the applied sound pressure. Thus the bulk viscosity is proportional to the imaginary part of the inverse of the frequency dependent adiabatic compressibility, $\beta(\omega)$ [39],

$$\zeta = \frac{\mathrm{Im}(1/\beta(\omega))}{\omega} \tag{10}$$

where ω is the angular frequency ($= 2\pi f$). Assuming a simple Debye relaxation model for $\beta(\omega)$ [39]:

$$\beta(\omega) = \beta_\infty + \frac{\beta_0 - \beta_\infty}{1 + \mathrm{i}\omega\tau} \tag{11}$$

one can introduce the relaxation time τ, which is a measure of the delay time for the volume change after the sound pressure. Here β_0 is the static adiabatic compressibility ($\beta_0 = 1/\rho v^2$) and β_∞ is the adiabatic compressibility at frequencies beyond the radio frequency range. putting equation (11) into equation (10) we obtain the following expression of the bulk viscosity:

$$\zeta = \frac{(\beta_0 - \beta_\infty)\tau}{\beta_0^2 + \omega^2\tau^2\beta_\infty^2}. \tag{12}$$

Since the present acoustic measurements are made in the radio frequency range, we may assume

$$\omega\tau \leqslant 1. \tag{13}$$

Then equation (12) can be simplified as (see equation (21) of [39])

$$\zeta \simeq \frac{\beta_0 - \beta_\infty}{\beta_0^2}\tau. \tag{14}$$

Furthermore, since $\beta_\infty \geqslant 0$, it follows that

$$\tau \geqslant \beta_0\zeta. \tag{15}$$

Figure 10(a) illustrates a range of τ that satisfies the inequality (15) denoted by the solid line and the inequality (13) denoted by the dashed line. Here we have assumed that the bulk viscosity contribution to α can be expressed by the Gaussian function mentioned in section 3. It is evident from the figure that τ is considerably longer than a typical time scale (picosecond) [40] of the individual atomic motion in the liquid state. This may imply that the M–NM transition gives rise to slow dynamics.

Various mechanisms have been proposed to explain anomalous increase in the bulk viscosity and most of them are concerned with the relaxation in some kind of two-state system [39]. In molecular liquids, which have internal degrees of freedom, the internal effects such as the rotational isomeric are the major causes of the bulk viscosity [39]. Even in the monatomic liquids having no internal degree of freedom bulk viscosity is expected to arise if local structural rearrangements are induced with a finite relaxation time by the application of sound pressure [39].

If one considers a liquid as a mixture of two structural states with different molar volumes (V_1 and V_2) and different free energies, its bulk viscosity ζ may be written for frequencies well below the structural relaxation frequencies (i.e. $2\pi f\tau \ll 1$) [39],

$$\zeta = \frac{V x_1 x_2 \tau}{RT\beta_0^2}\left(\frac{\Delta V}{V}\right)^2 \tag{16}$$

where x_1 and x_2 ($= 1 - x_1$) are the mole fraction of the states 1 and 2, respectively. The total molar volume V is expressed as $x_1V_1 + x_2V_2$, and the volume difference ΔV is $V_1 - V_2$. To derive equation (16) we have used equation (14). If we fix the variables other than x_1 and x_2, ζ has the maximum value for $x_2/x_1 = \sqrt{V_1/V_2}$. Putting this value and experimentally estimated values such as ζ, β_0, V etc for liquid Hg at 8.3 g cm^{-3}, where the Gaussian function has the maximum, into equation (16), we obtain a relation between τ and $\Delta V/V$, as shown by the bold line in figure 10(b). The line should be truncated at both ends because τ should be shorter

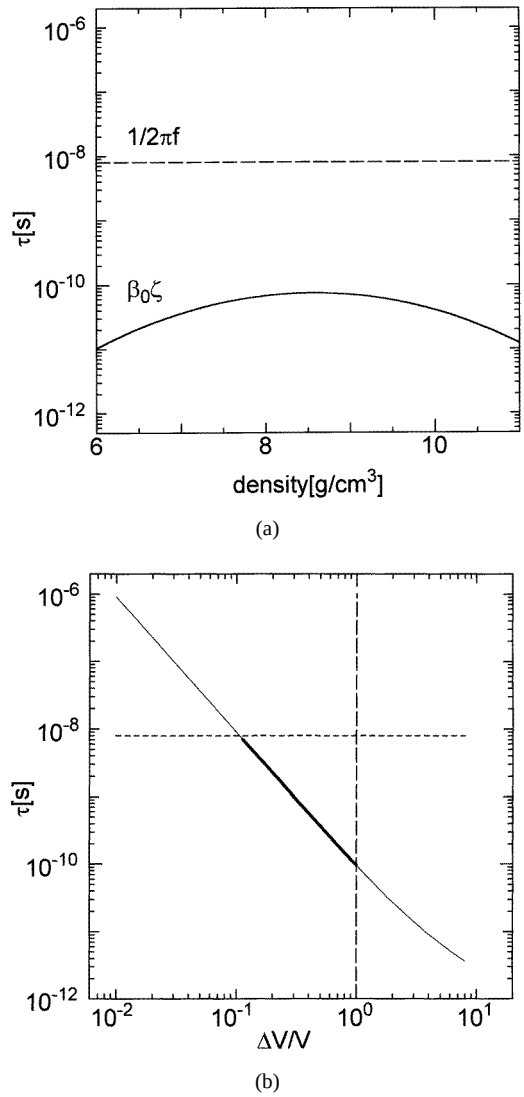

Figure 10. (a) The range of the relaxation time, τ, is shown against the density. It is bounded by the solid line, corresponding to the inequality (15), and by the dashed line, corresponding to the inequality (13). (b) The logarithm of the relaxation time, τ, estimated from equation (16) is plotted against the logarithm of the relative volume change, $\Delta V/V$. τ may lie within the range shown by the bold line. The dotted line and the dashed line correspond to $\tau = 1/2\pi f$ and $\Delta V/V = 1$, respectively.

than $1/2\pi f$ ($= 8.0$ ns) and $\Delta V/V$ should be smaller than unity. The latter corresponds to $\tau > 0.1$ ns, which nearly coincides with the maximum value of $\beta_0\zeta$ in figure 10(a). It should be noticed, however, that $\Delta V/V \geqslant 0.1$ even for the largest value of τ. Although the structural study by Tamura and Hosokawa [20] suggests that the nearest neighbour distance r_1 is elongated near the M–NM transition density, the relative dilatation, $\Delta r_1/r_1$, is less than 1%. Hence it seems unphysical that such a large change in $\Delta V/V$, as shown in figure 10(b), would be induced by the application of weak sound pressure.

An alternative way to interpret the present anomalous sound attenuation may be to introduce the changes in the electronic degrees of freedom by the sound pressure. Franz [12] proposed a simple model for the M–NM transition of expanded liquid Hg, in which she emphasized the importance of fluctuations in the local coordination number. In connection with this argument she demonstrated a possibility that in a tight-binding picture the removal of a single atom from a metallic Hg cluster changes the whole cluster into nonmetallic (see figure 1 of [12]). This study encourages us to assume that even a very small volume change induced by the applied sound pressure could lead to a drastic change in the electronic properties at the M–NM transition. When a local area or a cluster of Hg atoms is switched from nonmetallic to metallic by the sound pressure, it may be stabilized due to the metallic cohesion and remain metallic for a short time even after the sound pressure is removed. The switching from nonmetallic to metallic and *vice versa* may be regarded as a two-state system. The fact that the anomalous sound attenuation in the M–NM transition range depends little on temperature may also support the idea that the present two-state system is closely related to the changes in the electronic degrees of freedom. Electronic theory of the sound propagation in liquids is highly required.

5. Summary

The sound attenuation coefficient α of fluid mercury has been measured at 20 MHz in the temperature and pressure range up to 1600 °C and 200 MPa with four different sample lengths. As well as a sharp increase in α due to the critical attenuation, a secondary maximum has been observed in the density dependence of α in the M–NM transition range. The height of the secondary maximum depends very little on temperature in sharp contrast to the critical attenuation. Assuming Debye-type relaxation for the adiabatic compressibility, we have estimated the relaxation time and concluded that the M–NM transition gives rise to slow dynamics in expanded liquid Hg. We are now extending the acoustic measurements for liquid Hg to various frequencies other than 20 MHz, which may enable us to determine the relaxation time more precisely and to discuss the attenuation mechanism in more detail.

Acknowledgments

The authors are grateful to Dr K Okada, Messrs A Odawara, Y Kajihara, Y Hiejima and N Itokawa for collaboration on the experiments. We also thank Professors H Endo, F Hensel and K Tamura for valuable discussions. This work was partially supported by a Grant-in-Aid for Scientific Research on Priority Areas 'Physics of complex liquids' from the Ministry of Education, Science, Sports and Culture, Japan.

References

[1] Ikezi H, Schwarzenegger K, Simons A L, Passner A L and McCall S L 1978 *Phys. Rev.* B **18** 2494
[2] Hefner W, Schmutzler R W and Hensel F 1980 *J. Physique Coll.* **41** C8 62
[3] Yao M, Hayami W and Endo H 1990 *J. Non-Cryst. Solids* **117/118** 473
[4] Yao M 1994 *Z. Phys. Chem.* **184** 73
[5] Hensel F and Frank E U 1966 *Ber. Bunsenges. Phys. Chem.* **70** 1154
[6] Schmutzler R W and Hensel F 1972 *Ber. Bunsenges. Phys. Chem.* **76** 53
[7] Schönherr G, Schmutzler R W and Hensel F 1979 *Phil. Mag.* B **40** 411
[8] Yao M and Endo H 1982 *J. Phys. Soc. Japan.* **51** 966
[9] Even U and Jortner J 1972 *Phil. Mag.* **25** 715
[10] Warren W W Jr and Hensel F 1982 *Phys. Rev.* B **26** 966

[11] Mattheiss L F and Warren W W Jr 1977 *Phys. Rev.* B **16** 624
[12] Franz J R 1986 *Phys. Rev. Lett.* **57** 889
[13] Kresse G and Hafner J 1997 *Phys. Rev.* B **55** 7539
[14] Tamura K and Hosokawa S 1993 *J. Non-Cryst. Solids* **156–158** 646
[15] Endo H, Tamura K and Yao M 1987 *Can. J. Phys.* **65** 266
[16] Suzuki K, Inutake M, Fujiwaka S, Yao M and Endo H 1980 *J. Physique Coll.* **41** C8 66
[17] Kozhevnilov V F, Naurzakov S P and Arnold D I 1993 *J. Moscow Phys. Soc.* **3** 191
[18] Yao M, Okada K, Aoki T and Endo H 1996 *J. Non-Cryst. Solids* **205–207** 274
[19] Okada K, Odawara A and Yao M 1998 *Rev. High Pressure Sci. Technol.* **7** 736
[20] Tamura K and Hosokawa S 1998 *Phys. Rev.* **58** 9030
[21] Munejiri S, Shimojo F and Hoshino K 1998 *J. Phys.: Condens. Matter* **10** 4963
[22] Tamura K and Hosokawa S 1994 *J. Phys.: Condens. Matter* **6** A214
[23] Kozhevnikov V, Arnold D, Grodzinskii E and Naurzakov S 1996 *J. Non-Cryst. Solids* **205–207** 256
[24] Kohno H, Okada K, Kajihara Y, Hiejima Y and Yao M 1999 *J. Non-Cryst. Solids* at press
[25] Kohno H and Yao M in preparation
[26] Götzlaff W 1988 *PhD Thesis* University of Marburg
[27] Kozhevnikov V F, Arnold D I, Naurzakov S P and Fisher M E 1997 *Phys. Rev. Lett.* **78** 1735
[28] Yao M and Hensel F 1996 *J. Phys.: Condens. Matter* **8** 9547
[29] Ohmasa Y, Kajihara Y and Yao M 1998 *J. Phys.: Condens. Matter* **10** 11 589
[30] Postill D R, Ross R G and Cusack N E 1968 *Phil. Mag.* **18** 519
[31] Yao M, Takehana K and Endo H 1996 *J. Non-Cryst. Solids* **205–207** 270
[32] Dladla B S, Pilgrim W-C and Hensel F 1997 *Z. Phys. Chem.* **199** 295
[33] See Hansen J-P and McDonald I R 1986 *Theory of Simple Liquids* 2nd edn (London: Academic) ch 8
[34] Hunter J L, Welch T J and Montrose C J 1963 *J. Acoust. Soc. Am.* **35** 1568
[35] Tippelskirche H v, Franck E U and Hensel F 1975 *Ber. Bunsenges. Phys. Chem.* **79** 889
[36] See Kittel C 1986 *Introduction to Solid State Physics* 6th edn (New York: Wiley) ch 6
[37] Levin M and Schmutzler R W 1984 *J. Non-Cryst. Solids* **61/62** 83
[38] Kohno H and Yao M in preparation
[39] Litovitz T A and Davis C M 1965 *Physical Acoustics* vol II, ed W P Mason (New York: Academic) ch 5
[40] Hansen J-P and McDonald I R 1986 *Theory of Simple Liquids* 2nd edn (London: Academic) p 217